ISSN : 0974 - 7486 Volume 9 Issue 6

Trade Science Inc.

Materials Science

An Indian Journal

Full Paper

MSAIJ, 9(6), 2013 [209-216]

Comparative XRD, XRF and SEM studies of phase compositions and elemental distributions for Fe, Co-containing catalysts

Mai M.Khalaf[1]*, H.C.Ibrahimov[2], E.H.Ismailov[2], Y.H.Yusifov[2], N.M.Alieva[2]

[1]Chemistry Department, Faculty of Science, Sohag University, 82524 Sohag, (EGYPT)

[2]Institute of Petrochemical Processes, Azerbaijan National Academy of Sciences 30, Khojaly Ave., Baku, AZ1025, (AZERBAIJAN)

E-mail: mai_kha1@yahoo.com

ABSTRACT

This paper is primarily focused on the characterization of iron and cobalt nanoscale oxides synthesized by a method based on reaction of fine-dispersed Al flakes with dichloroethane in paraffin medium in the presence of iron and cobalt chlorides at different calcined temperatures forming catalytic complexes. This chemical-based synthesis route is briefly described, and the feasibility of obtaining such oxides. Characterization was done by X-ray fluorescence microscopy (XRFM), X-ray diffractometer (XRD), and scanning electron microscopy (SEM) studies which revealed, respectively, the presence of oxides and their nanoscale structures, including the elemental distribution and mass thickness of the these elements over the layers.

KEYWORDS

Thermal treatment;
Fe;
Co-containing catalysts;
XRFM;
XRD;
SEM.

INTRODUCTION

Transition metals provide a distinct advantage over precious metals because of their decreased costs. Interest in iron nanoparticles originates from iron's magnetic properties, its ready availability and low cost, and its high reactivity, particularly in reducing atmospheres[1-7]. Iron oxides in nano-scale have exhibited great potential for their applications as catalytic materials, pigments, flocculants, coatings, gas sensors, ion exchangers, magnetic recording devices, magnetic data storage devices, toners and inks for xerography, magnetic resonance imaging, bio separation and medicine No long-range magnetic order was detected in $FeAl_2O_4$, although the magnetic susceptibility reveals a maximum close to 12 K[8]. The preparation of $FeAl_2O_4$ is gaining importance due to its potential application as a magnetic material. However, most of the studies have been done on bulk samples and there are almost no reports on nanocrystalline $FeAl_2O_4$. cobalt oxides (CoO and Co_3O_4) have received a widespread attention due to their appealing multi-functional properties of technological interest. To this regard, actual challenging issues concern the devising and optimization of synthetic strategies towards high purity nanomaterials with specific features, opening new frontiers not only for understanding their fundamental properties, but also for developing new generation nanodevices with improved performances[9-14]. The literature is replete with synthetic routes to cobalt oxides, and cobalt-containing materi-

als especially for compositions along the CoO_x–Al_2O_3 systems. The standard method is via a solid-state reaction of the parent oxides. Other synthesis methods include sol–gel[15,16], co-precipitation[17,18], hydrothermal[19], polymeric precursor[20] and vapor deposition processing[21]. In this work our study is focused on increasing the activity of the nanostructured alumina materials by modifying it in the mode of «in situ» with metal chlorides of Fe (III) and Co (II) under laboratory conditions and after thermal treatment to produce new phases of the formed catalytic systems to be applicable in different fields as mentioned above. To identify the nature of active sites of the catalyst system and the different oxides which formed in our system after different calcinations, it has been investigated using the methods of X-ray diffractometer (XRD), X-ray fluorescence microscopy (XRF) and scanning electron microscopy (SEM).

EXPERIMENTAL

Synthesis of the alumina matrices containing Fe^{III}, Co^{II} ions

The alumina matrices containing Fe^{III} and Co^{II} ions were synthesized depending on the interaction of aluminum with dichloroethane as a catalytic complex CTC modified with metal chlorides of Fe (III) and Co (II)[22] in laboratory conditions under atmospheric pressure in a solvent in the mode of «in situ», at a certain ratio of initial components in a round bottom flask (reflux system) at temperature 75-80 °C for 22-25h. The obtained gel was dried at 100-110°C. The obtained dried xerogels (designated as Fe/CTC -110, Co/CTC-110) was submitted to thermal treatment at 400, 600, and 850°C for 2h, 4h in air, furnishing the materials designated as following:

complexes	400 °C	600 °C	850 °C
Fe/CTC	Fe/CTC- 400	Fe/CTC- 600	Fe/CTC- 850
Co/CTC	Co/CTC- 400	Co/CTC- 600	Co/CTC- 850

RESULTS AND DISSCUSSION

X-ray fluorescence microscopy (XRFM) characterization

Elemental analysis of the samples was performed by using X-ray microscope XGT-7000, Horiba with accelerating voltage of X-ray tube 50KV. For samples after calcinations at 400,600,850 °C for 2h in air as shown in TABLE 1, at 400 °C the distribution and mass thickness of chloride decreased due to the decomposition of Cl, reports on decomposition of nickel chlorides were given by others[23] and stated that decomposition characteristics depend on initial ingredient. The percentage of the chemical composition of the samples given in oxides at different calcined temperatures has not a distinct behavior; it depends on the stability of the formed oxides. For the complex CTC modified with iron chloride the red ferric oxide mixed with black ferrious oxide were formed at 400 °C, after calcinations at 600 and 850 °C in air for two and four hours for this complex the iron (II) aluminate, Al_2FeO_4 phase was formed. While for the other complex CTC modified with cobalt chloride the cobalt (II) aluminate ($CoAl_2O_4$) phases was formed mixed with grayish cobalt (II) and (III) oxides as shown in Figures 2. For the volatile materials percentage at calcined temperatures has the following arrangement Fe/CTC<Co/CTC and for ash% has the opposite arrangement that is refers to the reaction conditions. The data in TABLE 2 showed that, there are no change in the chemical composition and the distribution of elements for the investigated complexes after calcinations at 600 °C for the Fe/CTC, this means that the formed oxides at this temperature of higher stability. Also it has been observed that the percentage of the chemical composition of Fe_xO_y for the Fe/CTC complex decrease in the case of calcination for 4h than those obtained after 2h. This due to, the Fe/CTC complex formed mixed oxides of iron in the case of calcination for 2h, but after 4 hours the stable oxide of iron was remained. Also it was observed that the percentage of the chemical composition of CoO_x for the Co/CTC complex increase in the case of calcination for 4h than those obtained after 2h with regard to the percentage of Al_xO_y. This due to, the Co/CTC complex formed Co_3O_4 phase which is more stable than the CoO or Co_2O_3 phase below 925 °C in air[24]. From the optical image (Figure1, 2), it was observed that the color of the Fe/CTC and Co/CTC complexes changed by changing in the formed phases, these results were confirmed by XRD which will be discussed later. The distribution of the Co and Fe elements over depth at

the different calcined temperatures are higher than that of Al element that is for the higher synthetic ratio of cobalt and iron chlorides rather than Al flakes. Also the distribution of Co and Fe elements at 600 ˚C are higher than its distribution at other calcined temperatures due to the mixed oxides which are formed at 600 ˚C.

TABLE 1 : The elemental and chemical composition of the samples and their distribution of elements over the depth after calcinations in air: 400, 600, 850 °C for 2h.

Samples name	Chemical composition (wt. %)				Elements (wt. %)						Volatile %	Ash %	The distribution of elements over the depth			
	Al_xO_y	Fe_xO_y	CoO_x	Cl	Al	*C	Fe	Co	O	Cl			Al	Fe	Co	Cl
Fe/KTK-400	46.6	49.4	-	4.1	23.6	4.1	33.1	-	35.3	3.9	53	46.9	0.212	0.361	-	0.018
Co/KTK-400	58.2	-	27.9	5.4	29.5	2.8	-	19.8	34.1	5.0	63.4	36.7	0.028	-	0.133	0.011
Fe/KTK-600	34.9	64.2	-	0.9	17.9	3,9	43.6	-	34.6	0.8	63.2	36.8	0.038	0.773	-	-
Co/KTK-600	67.6		32.4	0.7	33.8	5.4	-	24.1	36.7	0.6	77.2	22.7	0.032	-	0.213	-
Fe/KTK-850	66.5	33.5		-	33.8	3.9	22.5		39.7	-	57.5	42.5	0.175	0.267		-
Co/KTK-850	78.7	-	21.3	-	39.4	5.4	-	15.8	39.3	-	66.7	33.3	0.134	-	0.175	-

TABLE 2 : The elemental and chemical composition of the samples and their distribution of elements over the depth after calcinations in air: 600,850 °C for 4h.

Samples name	Chemical composition(wt. %)			Elements (wt. %)					Volatile %	Ash %	The distribution of elements over the depth		
	Al_xO_y	Fe_xO_y	CoO_x	Al	*C	Fe	Co	O			Al	Fe	Co
Fe/CTC -600	82.3	17.9	-	41.8	3.9	12.0	-	42.3	71.8	28.2	0.020	0.032	-
Co/ CTC-600	47.8	-	52.2	23.8	5.4	-	38.8	31.8	69.2	30.8	0.064	-	0.223
Fe/CTC -850	82.2	17.8	-	41.8	3.6	12.0	-	42.3	73.5	26.5	0.014	0.027	-
Co/ CTC -850	54.2	-	45.9	27	5.4	-	34.2	33.4	71.5	28.4	0.085	-	0.223

***C content was determined by the balance of the treatment of the samples at 400,600and 850°C for 2h, 4h.**

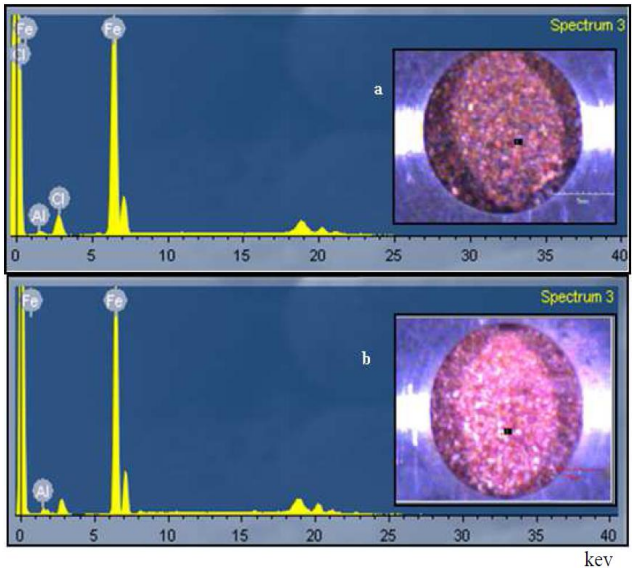

Figure 1 : EDRF analysis and optical image of (a) Fe/CTC-400 for 2h (b) Fe/CTC - 850 for 4h in air.

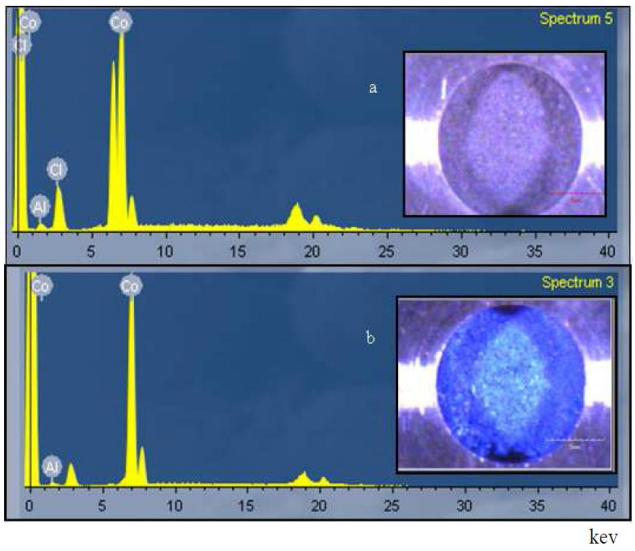

Figure 2 : EDRF analysis and optical image of (a) Co/CTC-400 holding complexes for 2h (b) Co/CTC-850 holding complexes for 4h in air.

X-ray diffraction (XRD) characterization

XRD patterns were obtained using TD-3500 diffractometer at room temperature. Diffraction patterns were obtained with none-filtered Cu Kα radiation (λ = 0.15418 nm), monochromatic X-ray beam, and X-ray tube parameters with 35 kv and 25 µA. To investigate the crystalline structure of the product, powder XRD measurements were taken at room temperature. The

Full Paper

X-ray diffraction patterns of the catalytic complexes Fe/CTC, Co/CTC obtained with thermal treatment at 850 ˚C for 2h and 4h in air are shown in Figure 3, 4, 5. Small angles XRD, SAXRD patterns of the same set of materials are inserted, and there are no characteristic peaks in this region. The patterns showed that, an amorphous structure was formed for the Fe/CTC complex at these treatments, but after calcinations at 850 ˚C for 2h crystalline phases were obtained as shown in Figure 3. The cubic Al_2O_3 was obtained for Fe/CTC and mixed phases of iron oxides FeO (2θ=61), synthetic magnetite $Fe^{+2}Fe^{+3}O_4$ (2θ=35°) and synthetic hematite Fe_2O_3 (2θ=23°, 33°, 49°, 54° and 64° files no. 06-0711, 19-0629 and 33-0664) were formed. Also the iron aluminates, $Fe^{+2}Al_2O_4$ phase was formed for the Fe/CTC, with characteristic peaks at 2θ=31°, 37°, 58°, and 65° (file no. 34-0192), the intensity of these peaks increases by increasing the calcined temperatures and by increasing the holding time of these complexes at the investigated temperatures. For the Co/CTC complex, the peaks in the wide angles are well indexed into cubic Al_2O_3 structure (file no. 29-0063). Three diffraction peaks observed at 2θ=37.4 °, 45.6 ° and 65.4 ° in both the samples corresponds to (311), (400) and (440) planes, respectively. Also the cobalt aluminates, $Co^{+2}Al_2O_4$ (file no. 10-0458) and Co_3O_4 phases (file no. 42-1467) were observed and showed peaks at 2θ=32 °,37 °, 39 °, 44.6 ° and 65 ° corresponds to (220), (311),(222), (400) and (440) planes. The phase composition changes gradually from cubic Al_2O_3 to Co_3O_4 and cobalt aluminates phases after thermal treatments of the samples at 600 and 850 ˚C. The broadening of powder XRD peaks indicates that the particle sizes are in nanometer range. Clearly, the peaks in Figure 5b are a little broader than that in Figure 5c indicates that the particles decreased in size after thermal treatments at higher temperatures. These broad peaks first appear at 400 ˚C Figure 5a in air for 2h and give way to sharper, better defined peaks as the correct stoichiometry is reached. The expected cubic CoO phase was not observed because the thermal treatments occurred in air -rich atmospheres. The excess oxygen favors the formation of Co 31, which in turn favors the formation of the spinel [Co(II)- Co_2(III)O_4] structure, which detected by XRD.

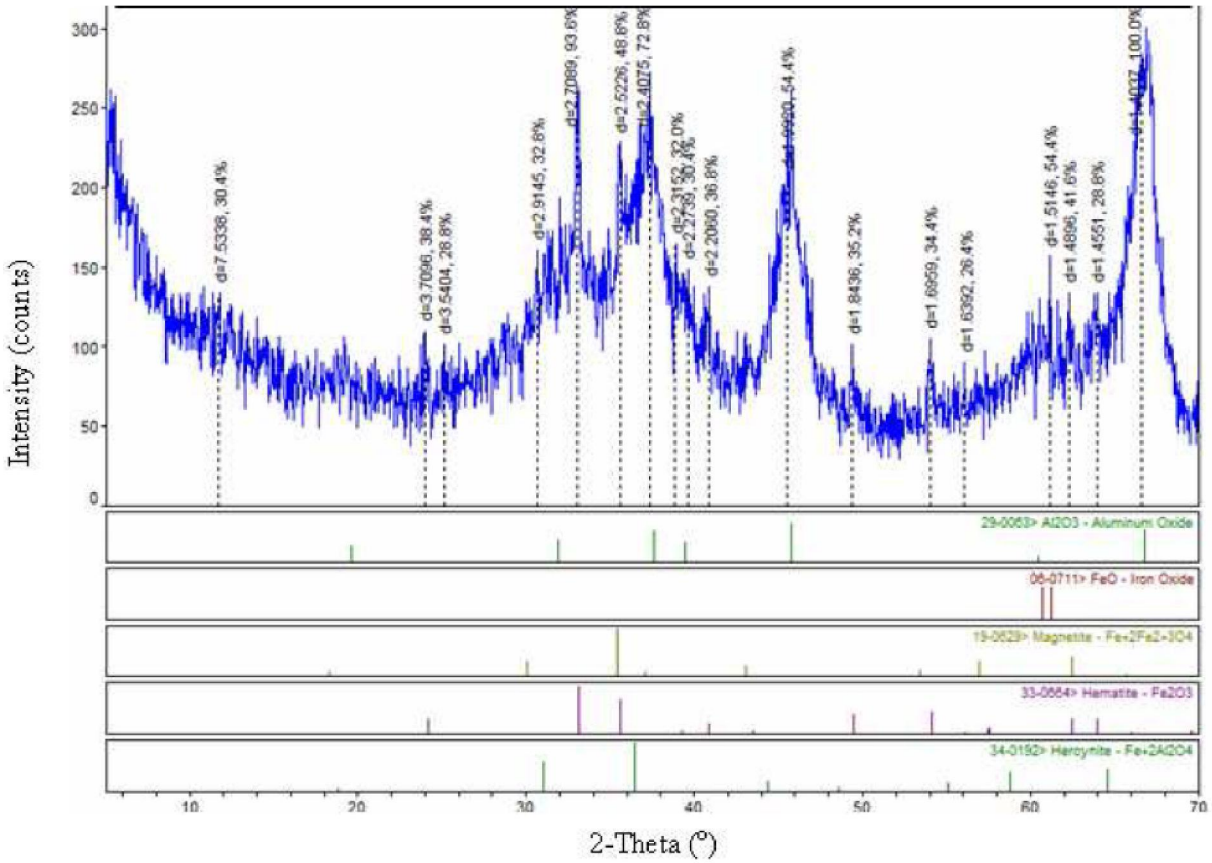

Figure 3 : XRD patterns of Fe/CTC at 850 °C in air for 2h.

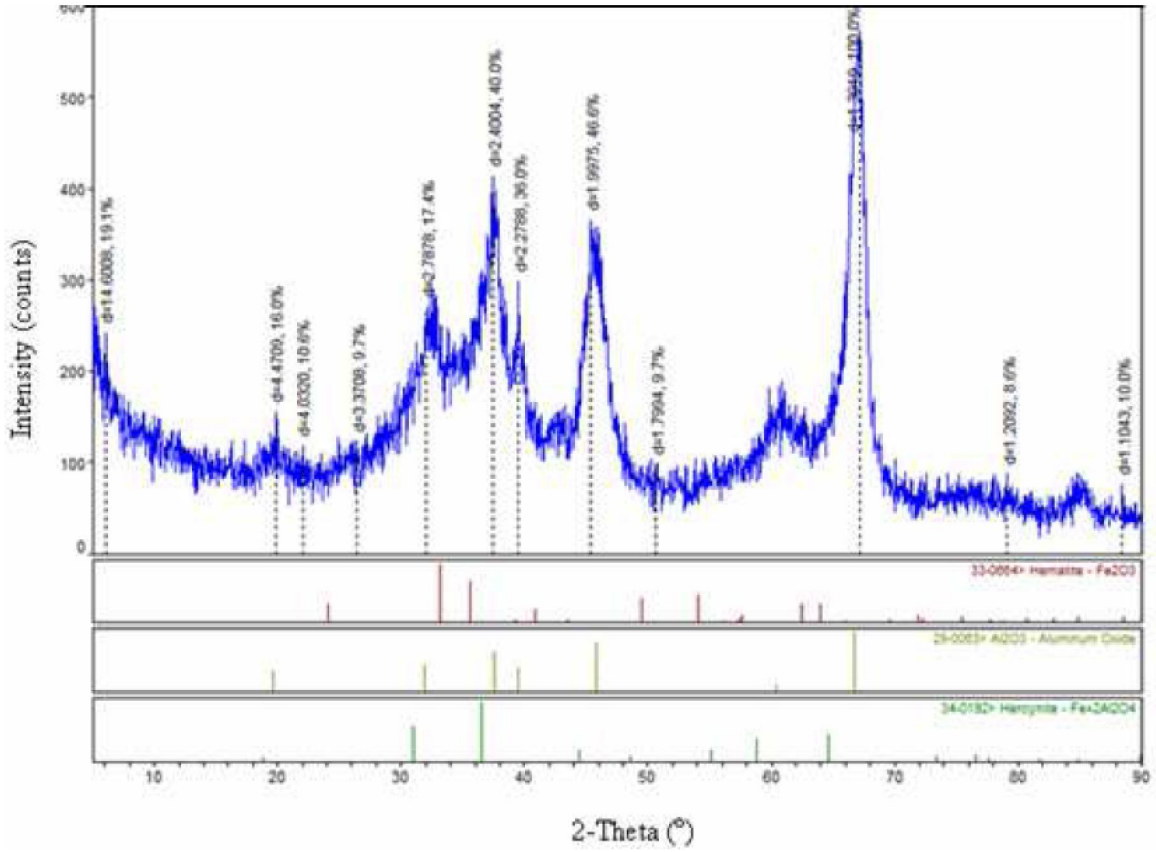

Figure 4 : XRD patterns of Fe/CTC at 850 °C in air for 4h.

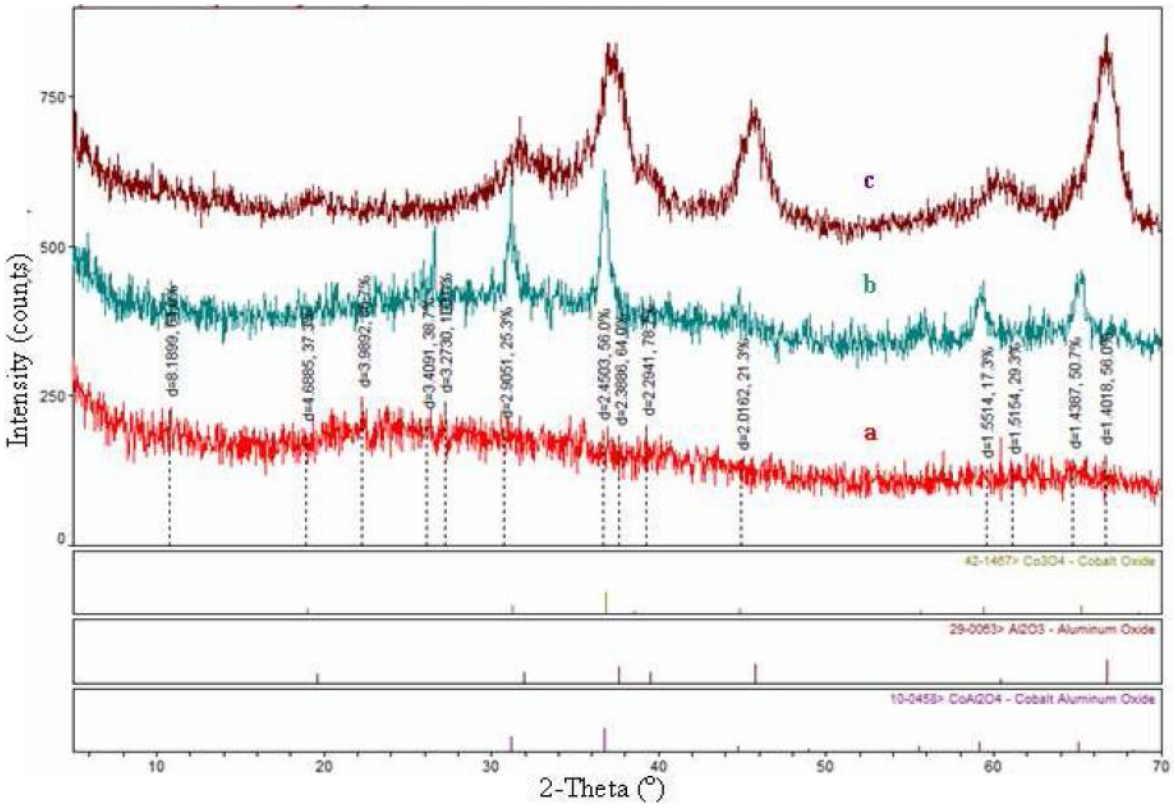

Figure 5 : XRD patterns of precursor samples Co/CTC for 2h in air (a) at 400 °C (b) at 600 °C (c) at 850 °C.

Full Paper

TABLE 3 : The values of the crystallite size of complexes after calcinations in air: 400, 600, 850 °C for 2h and 4h.

Complexes	Holding time	crystallite size (nm)		
		First peak	Second peak	Third peak
Co/CTC-200	2h	0.74	0.55	-
Fe/CTC-200	2h	0.81	1.02	-
Co/ CTC-400	2h	-	0.74	-
Fe/CTC-400	2h	-	0.97	-
Co/CTC-600	2h	4.7	3.2	2.6
Fe/CTC-600	2h	-	1.97	-
Co/CTC-850	2h	1.2	1.4	1.2
Fe/CTC-850	2h	4.7	1.3	1.5
Co/CTC-850	4h	1.7	1.6	1.5
Fe/CTC-850	4h	1.7	1.2	1.4

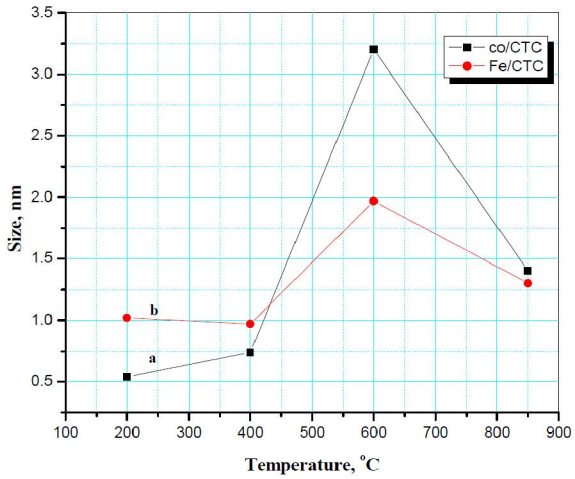

Figure 6 : Average size of (a) Co/CTC and (b) Fe /CTC complexes at various temperatures.

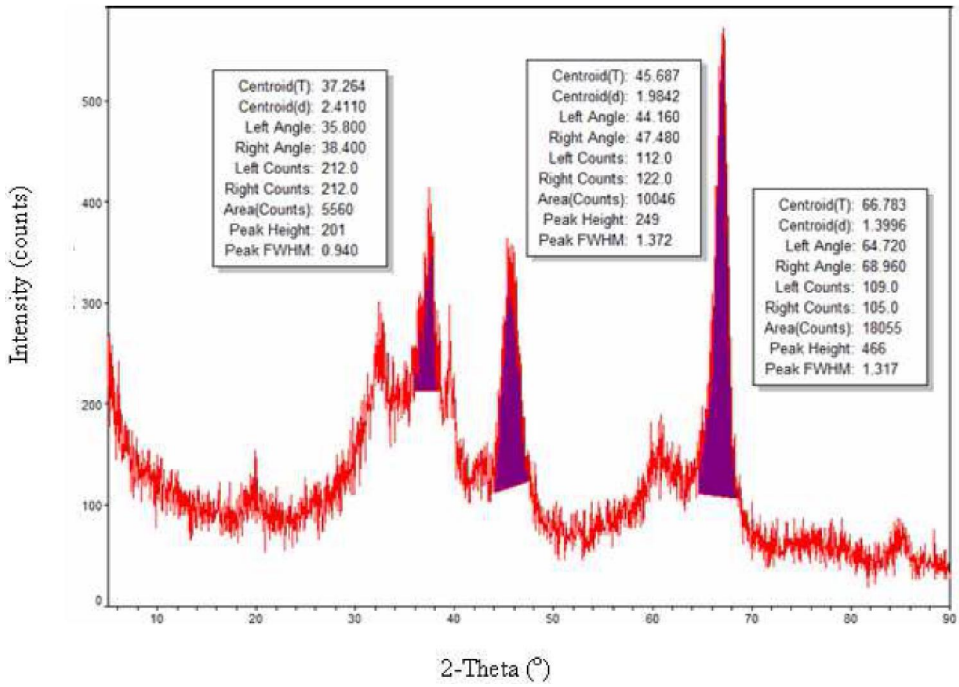

Figure 7 : XRD patterns of Fe/CTC at 850 °C in air for 4h for calculated grain size.

Crystallite size analysis

Crystallite size is directly related to the relevant physical and chemical properties of materials. Therefore, it's of great significance to measure the average grain size (primary aggregation) of materials. The average crystallite size was determined from the full width at half maxima (FWHM) of the diffraction peaks as shown in Figure 7 using Debye-Scherrer formula[25-27].

$$D = \frac{K\lambda}{\beta \cos\theta} \quad (1)$$

Where λ is the wave length of the x-rays, β is the full width at half maximum of the peak, θ is the Bragg's angle and K is the shape factor. According to the Scherrer formula, the calculated results for the average size of Fe/CTC and Co/CTC nanoparticles after thermal treatments at 200,400,600 and 850 ˚C are shown in Figure 6. The values are tabulated in TABLE 3 and the powder XRD analyses demonstrate a dramatic increasing trend of the grains size with the modification of the complex CTC with cobalt. Such increase of the size is attributed to the bigger size of Co atom in comparison to that of Fe atom. The size of Co/CTC complex increases slightly from 200 to 400 ˚C. After that

sharp increase to 3.2 nm at 600 ˚C, This indicates that at initial state at 200 ˚C the Al_2O_3 act as a barrier and prevented the oxidation of Co nanoparticles; after that at 600 ˚C, the phase of $CoAl_2O_4$ was formed mixed with Co_3O_4 and the average size of Co_3O_4 was bigger than the size of Co, since the Co nanoparticles were oxidized into Co_3O_4 [28]. However, the Al_2O_3 no longer acted as a barrier to effectively prevent the oxidation of Co. The size of the complex reduces signiûcantly at 850˚C, also the same trend was also obtained in case of the Fe/CTC complex which attributed to the formation of $Fe^{+2}Al_2O_4$ and $CoAl_2O_4$ phases which are more stable than other oxides, and this was notably observed from the chemical composition of the formed oxides of Fe_xO_y and CoO_x which decreased from 600 to 850˚C in air for 2h (TABLE 3). The same trend was obtained after thermal treatments from 600 to 850˚C in air for 4 hours.

SEM analyses

The morphology of the tested samples was observed by using scanning electron microscope (JEOL, model 5300). SEM analysis reveals that the synthesized iron and cobalt nanoparticles (Figure 8) are ranged in size from 50-100 nm with calculated average size of 100 nm. The images also reveal that there is no great modification was recognized for the morphology of the Fe particles. In fact similar aggregation and agglomeration which observed for Co particles were observed. There is a mixture of nanoparticles of iron, cobalt with spherical shape and aluminum oxides with rhombic shape and with different particle size as referred in images.

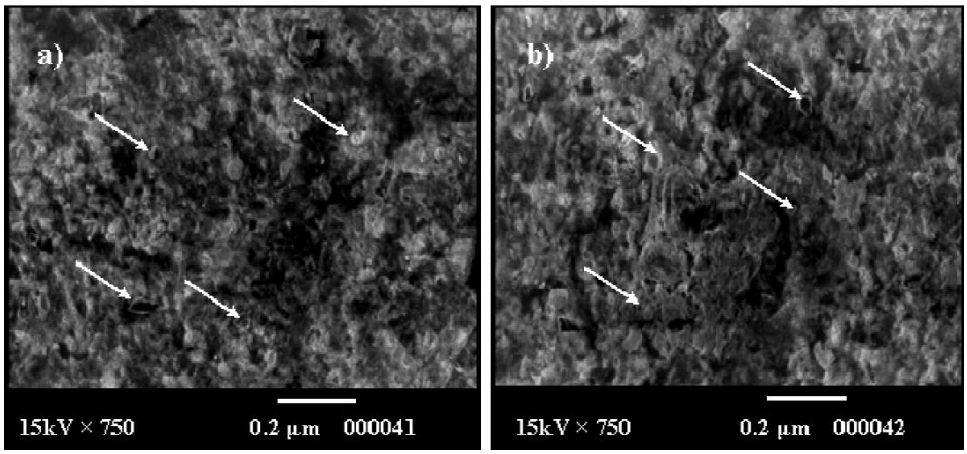

Figure 8 : SEM micrographs of samples a)Fe/CTC b)Co/CTC calcined at 850 °C in air for 4h.

COCLUSIONS

The following conclusions have been drawn from the present study:

1. This paper aims to introduce a unique process for preparing catalytic complexes of Fe/CTC and Co/CTC. This process requires only thermal treatments of these materials and uses low cost starting materials.
2. By the thermal treatments at different temperatures and different holding time we can control the methods of obtaining desired materials to be used in different applicable catalytic processes.
3. In this work it had been confirmed the synthesis and investigation of mixed iron oxides (FeO, $Fe^{+2}Fe^{+3}O_4$, Fe_2O_3) at 850 ˚C for 2h from the catalytic complex CTC modified using iron chloride by the characteristic techniques.
4. The same complex after calcinations at 850˚C for 4h we proposed the preparation of Fe_2O_3 and confirmed the presence of $Fe^{+2}Al_2O_4$ phase by XRFM and XRD.
5. The difference in the color of Fe/CTC complex from black color at 400˚C, then mixed color (black and brown) at 600˚C, then brown color at 850 ˚C for 2h after that light brown color at 850 ˚C for 4h, also for the cobalt phases at 600 ˚C of $CoAl_2O_4$ mixed with Co_3O_4, this difference confirmed the preparation of the different mentioned oxides.
6. The difference in the size of the catalytic complexes Co/CTC and Fe/CTC after heat treatment from 200 to 600 ˚C was due to the presence of Al_2O_3 as a barrier prevented the oxidation of Co and Fe

nanoparticles, this difference confirmed the presence of the different mentioned phases.

7. The increasing of temperature and time holding of these complexes lead to increase the intensity of XRD peaks, and this attributed to the increase in the degree of ordering of the particles.
8. SEM studies confirmed the presence of mixture phases of iron and aluminum oxides for Fe/CTC and cobalt and aluminum oxides for Co/CTC complexes.

REFERENCES

[1] S.Enthaler, K.Junge, M.Beller; J.Angew.Chem.Int. Ed.Engl., **47**, 3317 **(2008)**.

[2] A.B.M.Giasuddin, S.R.Kanel, H.Choi; J.Environ Sci.Technol., **41**, 2022 **(2007)**.

[3] K.T.Wu, P.C.Kuo, Y.D.Yao, E.H.Tsai; J.IEEE Trans.Magn., **37**, 2651 **(2001)**.

[4] A.N.Shipway, E.Katz, I.Willner; J.Chem.Phys. Chem., **1**, 18 **(2000)**.

[5] N.Tran, R.Pareta, E.Taylor, T.J.Webster; Adv.Mater.Res., **89**, 411 **(2010)**.

[6] B.Chertok, B.A.Moffat, A.E.David, F.Yu, C.Bergemann, B.D.Ross; J.Biomaterials., **29**, 487 **(2008)**.

[7] D.L.Huber; Small, **1**, 482 **(2005)**.

[8] N.Tristan, J.Hemberger, A.Krimmel, H.A.Krug von Nidda, V.Tsurkan, A.Loidl; J.Phys.Rev.B, **72**, 174404 **(2005)**.

[9] Y.Shao, J.Sun, L.Gao; J.Phys.Chem.C, **113**, 6566 **(2009)**.

[10] N.A.Barakat, M.S.Khil, F.A.Sheik, H.Y.Kim; J.Phys.Chem.C, **112**, 12225 **(2008)**.

[11] R.Xu, H.C.Zeng, J.Langmuir., **20**, 9780 **(2004)**.

[12] M.Verelst, T.O.Ely, C.Amiens, E.Snoeck, P.Lecante, A.Mosset, M.Respaud, J.M.Broto, B.Chaudret; J.Chem.Mater., **11**, 2702 **(1999)**.

[13] F.Gu, C.Li, Y.Hu, L.Zhang; J.Cryst.Growth., **304**, 369 **(2007)**.

[14] B.Varghese, T.C.Hoong, Z.Yanwu, M.V.Reddy, B.V.R.Chowdari, A.T.S.Wee, T.B.C.Vincent, C.T.Lim, C.H.Sow; J.Adv.Funct.Mater., **17**, 1932 **(2007)**.

[15] C.O.Arean, M.P.Mentruit, E.E.Platero, F.X.L.I.Xamena, J.B.Parra; Sol–gel method for preparing high surface area $CoAl_2O_4$ and Al_2O_3 – $CoAl_2O_4$ spinels. J.Mater.Lett., **39**, 22 **(1999)**.

[16] F.Meyer, A.Dierstein, C.Beck, W.Hartl, R.Hempelmann, S.Mathur, M.Veith; Size-controlled synthesis of nanoscaled aluminium spinels using heterobimetallic alkoxide precursors via water/oil microemulsions nanostruct. J.Mater., **12**, 71–74 **(1999)**.

[17] N.Ouahdi, S.Guillemet, J.J.Demai, B.Durand, L.Er.Rakho, R.Moussa, A.Samdi; Investigation of the reactivity of $AlCl_3$ and $CoCl_2$ toward molten alkali-metal nitrates in order to synthesize $CoAl_2O_4$. J.Mater.Lett., **59**, 334–340 **(2005)**.

[18] S.Chokkaram, R.Srinivasan, D.R.Milburn, B.H.Davis; Conversion of 2-octanol over nickel–alumina, cobalt–alumina, and alumina catalysts. J.Mol.Catal.A-Chem., **121**, 157–69 **(1997)**.

[19] Z.Z.Chen, E.W.Shi, W.J.Li, Y.Q.Zheng, J.Y.Zhuang, B.Xiao, L.A.Tang; Preparation of nanosized cobalt aluminate powders by a hydrothermal method. J.Mater.Sci.Eng.B-Solid., **107**, 217–223 **(2004)**.

[20] W.S.Cho, M.Kakihana; Crystallization of ceramic pigment $CoAl_2O_4$ nanocrystals from Co–Al metal organic precursor. J.Alloy Compounds, **287**, 87–90 **(1999)**.

[21] V.Dureuil, C.Ricolleau, M.Gandais, C.Grigis, J.P.Lacharme, A.Naudon; Growth and morphology of cobalt nanoparticles on alumina. J.Cryst.Growth, **233**, 737–748 **(2001)**.

[22] Kh.D.Ibragimov, E.G.Ismailov, G.S.Martynova, N.R.Bektashi, Z.M.Ibragimova, M.I.Rustamov; Synthesis of a component of the jet engine fuel and an accelerator of oil tar oxidation by catalytic processing of heavy pyrolysis tar. Russian Journal of Applied Chemistry, **83(7)**, 1159-1163 **(2010)**.

[23] A.F.Holleman, E.Wiberg; Inorganic chemistry. San Diego: Academic Press., ISBN 0-12-352651-5, **(2001)**.

[24] X.F.Zhang, X.L.Dong, H.Huang, B.Lv, X.G.Zhu, J.P.Lei, S.Ma, W.Liu, Z.D.Zhang; J.Acta Mater., **55**, 3727 **(2007)**.

[25] B.D.Cullity; Elements of x-ray diffraction, 2nd Edition, **(1978)**.

[26] J.Fang, K.L.Stokes, W.Zhou, J.A.Wiemann, J.Dai, C.J.O'Connor; ISCANI, World Scientific Publishing., **9**, **(2000)**.

[27] H.P.Klug, L.E.Alexander; X-ray differaction procedures for polycrystalline and amorphous materials, Wiley, New York, **(1954)**.

[28] X.G.Liu, D.Y.Geng, J.M.Liang, Z.D.Zhang; Magnetic stability of Al_2O_3 -coated fcc-Co nanocapsules. Journal of Alloys and Compounds, **465**, 8–14 **(2008)**.